THE DIFFERENCE BETWEEN

RADIO-LOUD and RADIO-QUIET

AGN

Marek Sikora

(with Lukasz Stawarz and Jean-Pierre Lasota)

Seeon, 2007

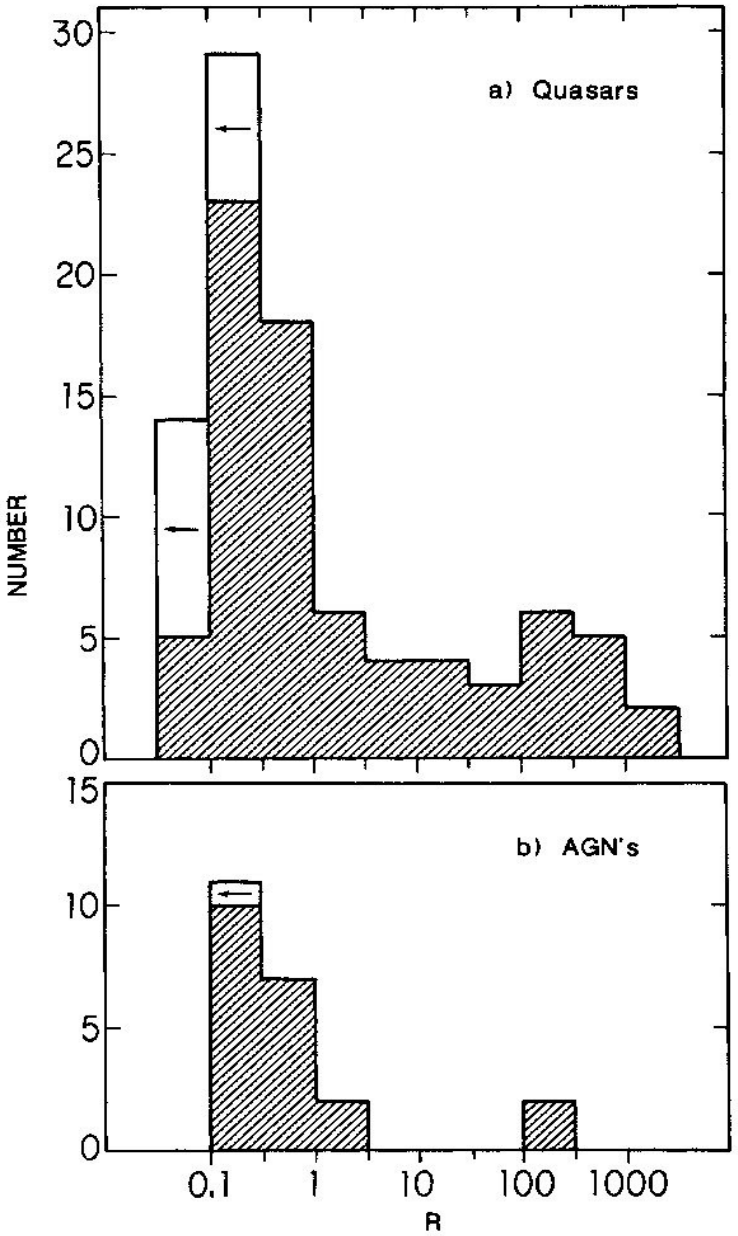

FIG. 5. Distribution of R for (a) 91 quasars in the BQS sample and (b) the 22 AGNs.

$$\mathcal{R} \equiv L_{\nu R}/L_{\nu O}$$

$$L_R \equiv \nu_R L_{\nu R},\ L_O \equiv \nu_O L_{\nu O}$$

$$L_R/L_O \sim 10^{-5}\mathcal{R}$$

Kellermann et al. '89

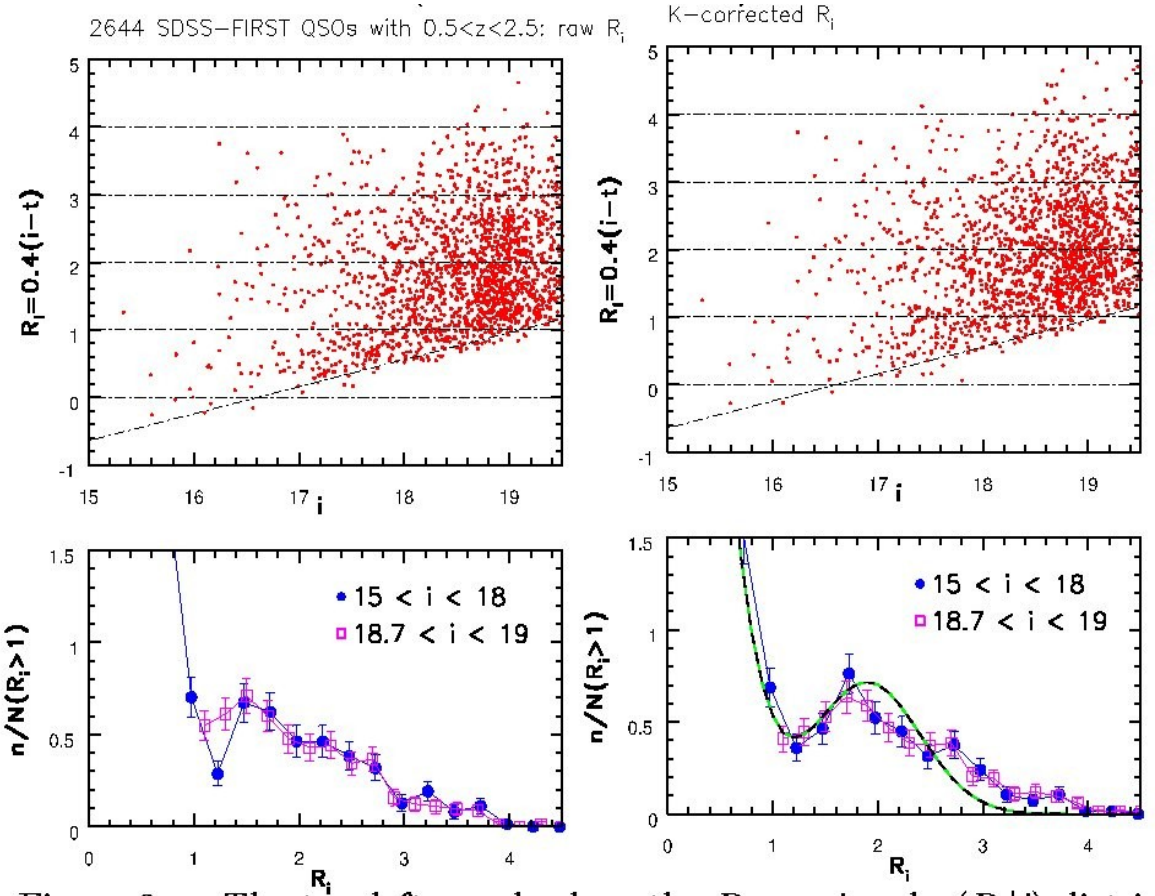

Figure 2. The two left panels show the R_i vs. i and $p(R_i|i)$ distributions for quasars with $0.5 < z < 2.5$ in two i magnitude bins, where R_i is **not** K-corrected. The two right panels show analogous results when R_i **is** K-corrected using eq. 1. The thick line in the bottom right panel is the best-fit using the same functional form as proposed by C03 (a double Gaussian). It has a local minimum at $R_i \sim 1.2$ and a local maximum at $R_i \sim 1.9$, with the maximum-to-minimum ratio of $\sim$2.

Ivezić et al. '03

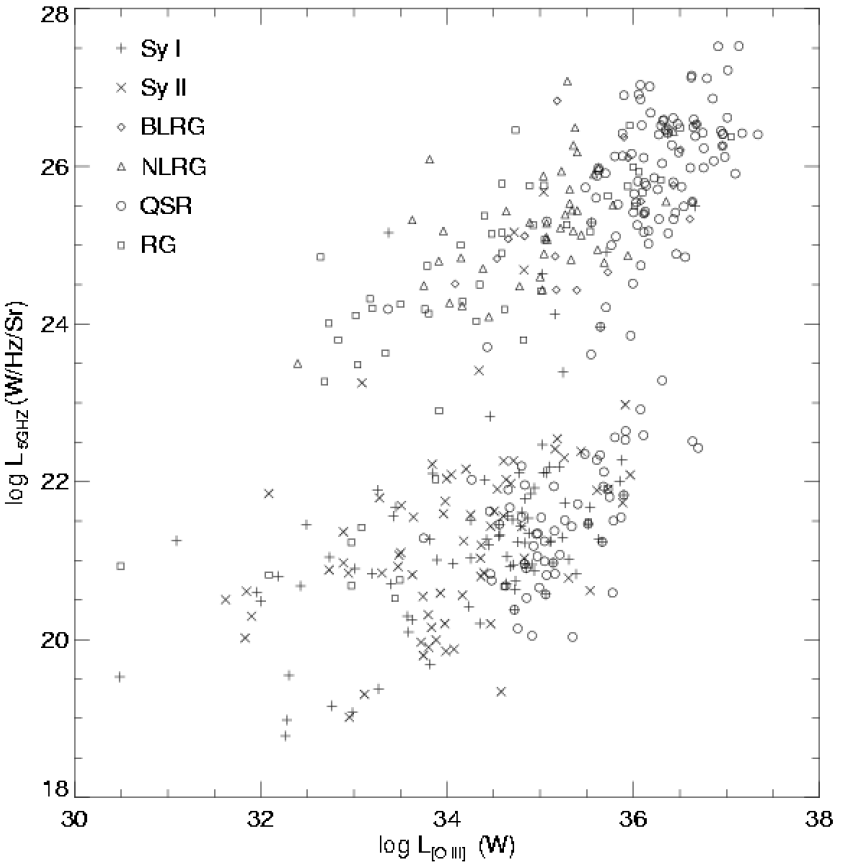
Sy I
Sy II
BLRG
NLRG
QSR
RG
log L5GHz (W/Hz/Sr)
log L[O III] (W)
28
26
24
22
20
18
30
32
34
36
38

Xu et al. '99

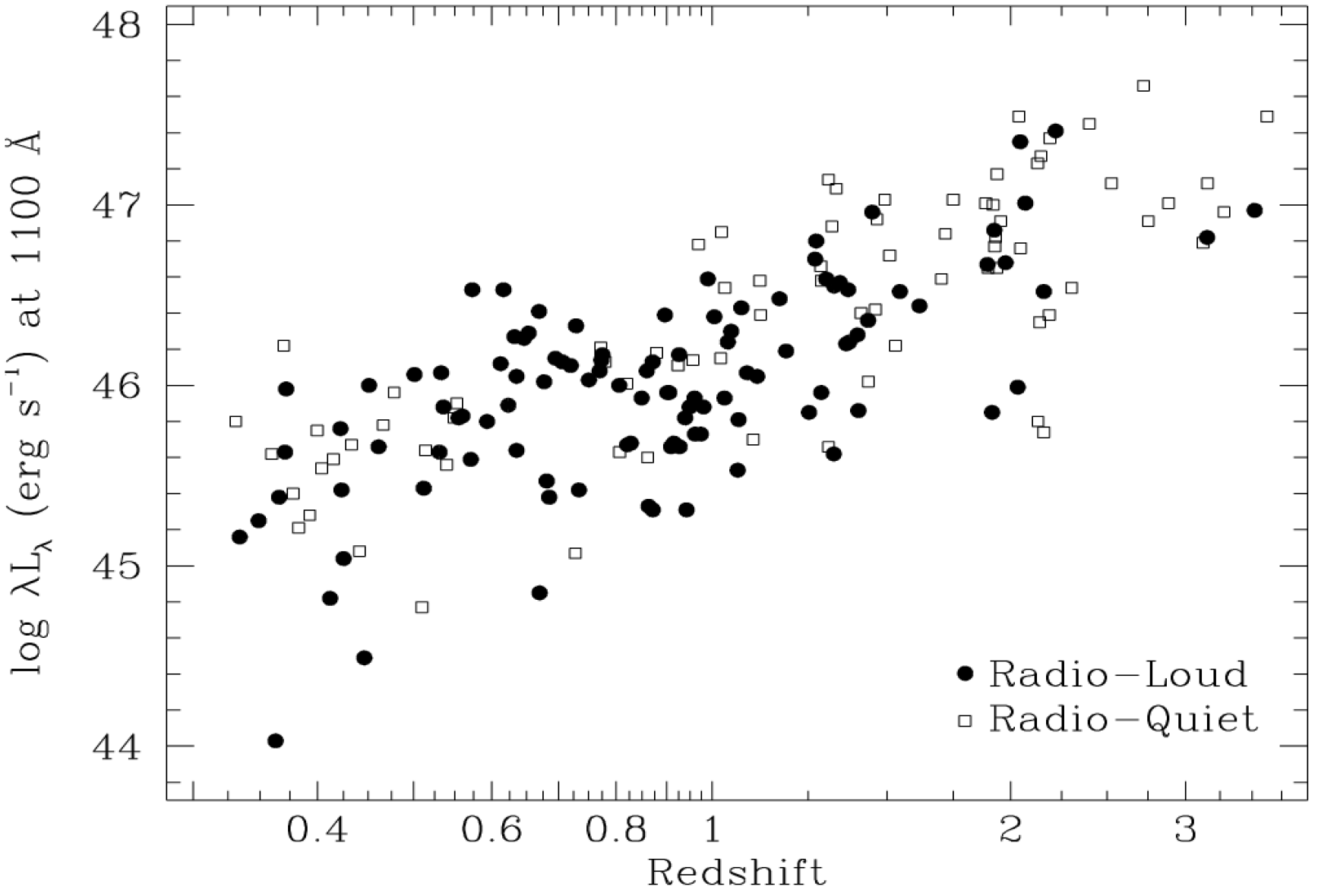

Telfer et al. '02

1989ApJ...347...29S

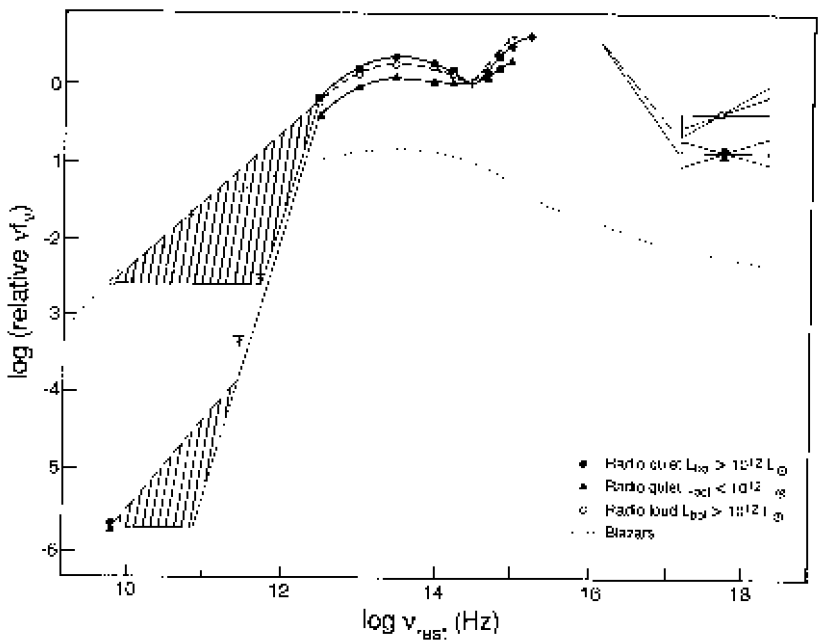

FIG. 2.—Average continuum energy distributions for radio-loud and radio-quiet PG quasars. The data points are mean values for the quasars in Fig. 1. Variations in the mean are typically 0.15 in the log for the far infrared data, and 0.1 in the log for the near-infrared and optical data. The X-ray slopes are adopted from Wilkes and Elvis (1987). The hatched region at radio-submillimeter wavelengths represents the range of spectral indices observed. Shown for comparison (*dotted line*) is the mean continuum energy distribution for blazars (Impey and Neugebauer 1988), normalized at 6 cm (see text).

Sanders et al. '89

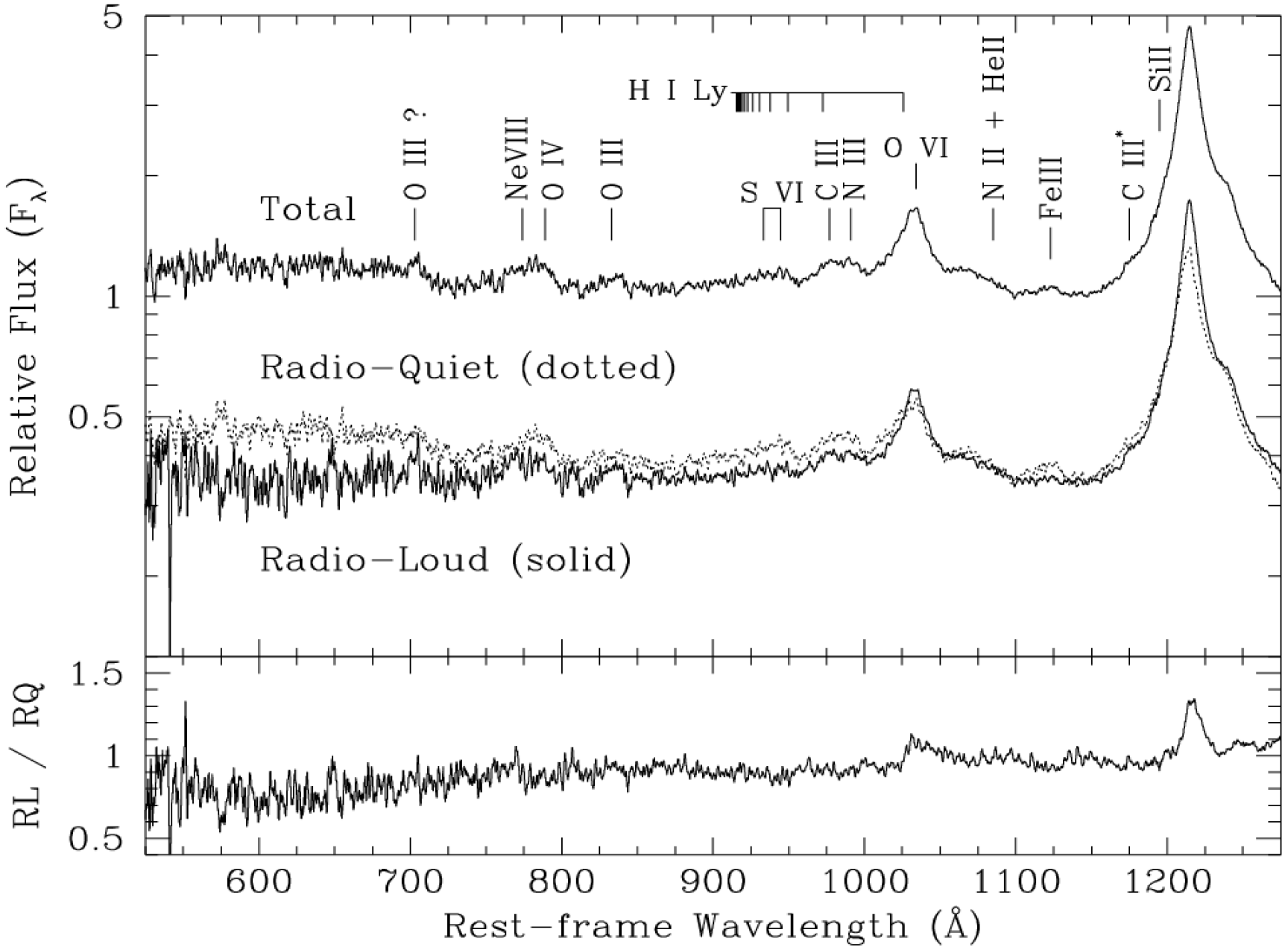

Telfer et al. '03

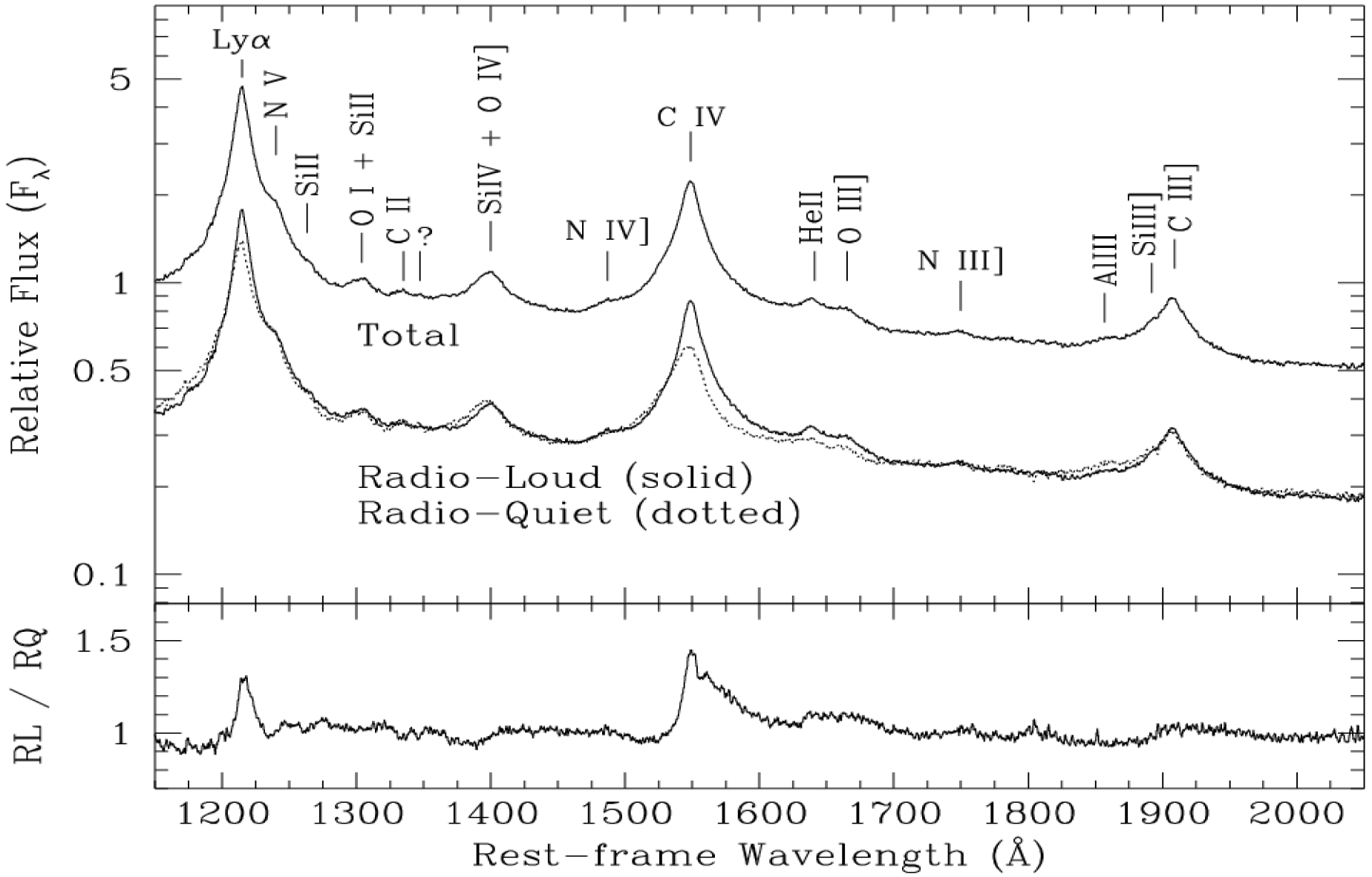

Tefler et al. '03

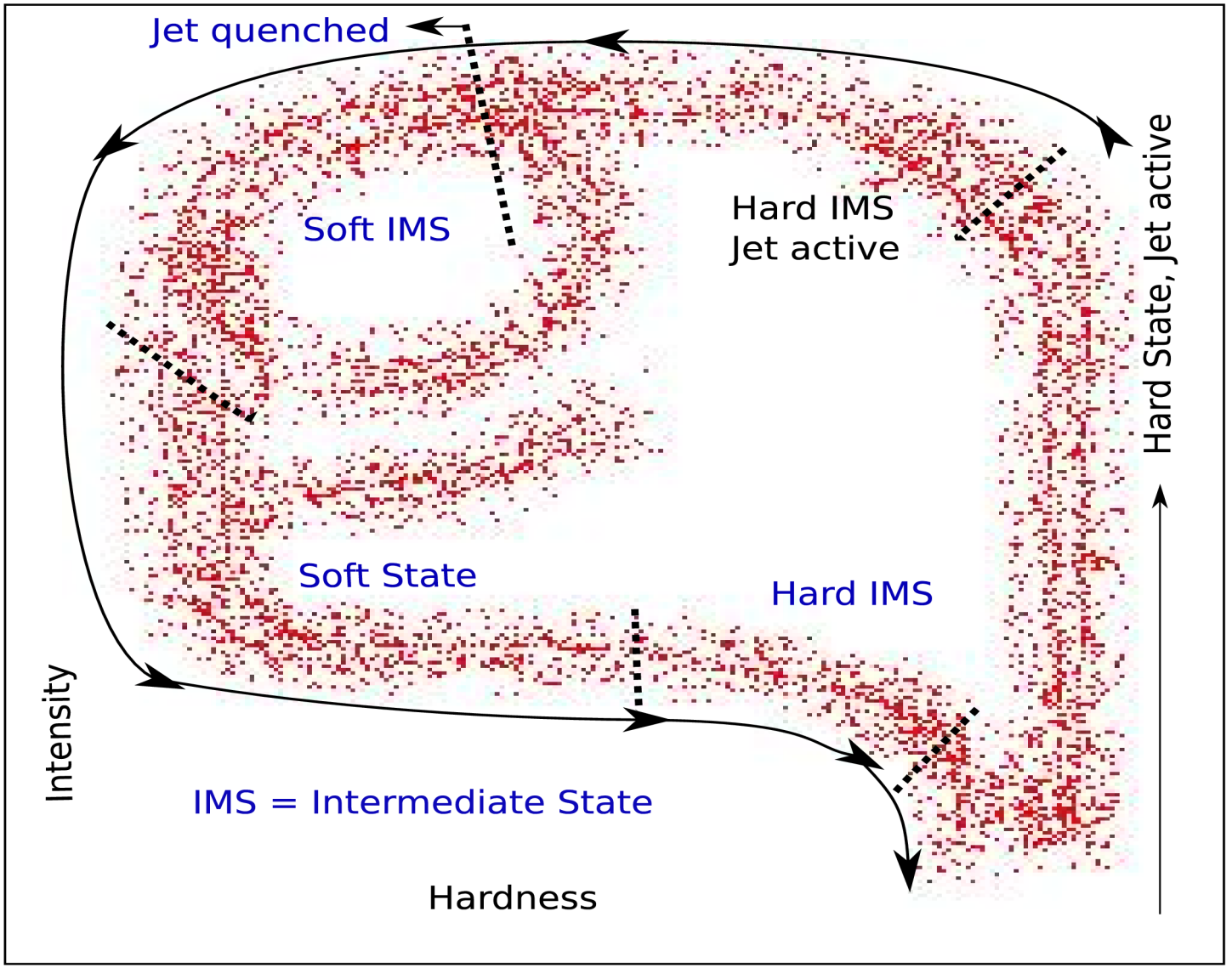

Kording et al. '06

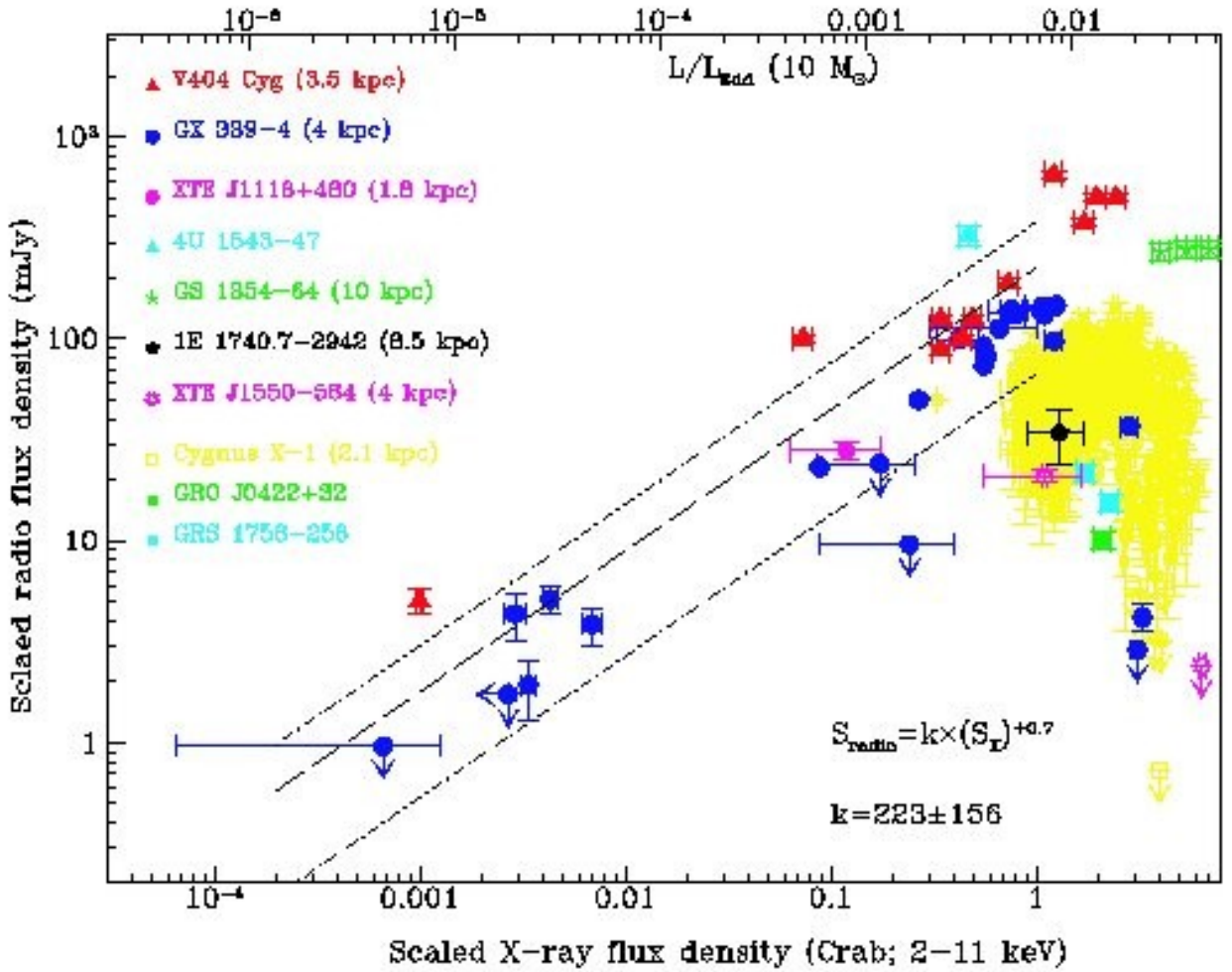

Figure 2. The radio flux density (mJy) is plotted against the X-ray flux density (Crab) for a sample of 10 hard state BHs (see Table 1), scaled to a distance of 1 kpc and absorption corrected (this means that the axes are proportional to luminosities). On the top horizontal axis we indicate luminosity, in Eddington units for a 10-$M_\odot$ BH, corresponding to the underlying X-ray flux density. An evident correlation between these two bands appears and holds over more than three orders of magnitude in luminosity. The dashed line indicates the best fit to the correlation, that is $S_{radio} = k(S_X)^{+0.7}$, with $k = 223 \pm 156$ (obtained by fixing the slope at +0.7, as found individually for both GX 339−4 and V404 Cygni; see Section 4.1). Errors are given at the 3σ confidence level and arrows also represent 3σ upper limits.

Gallo et al. '03

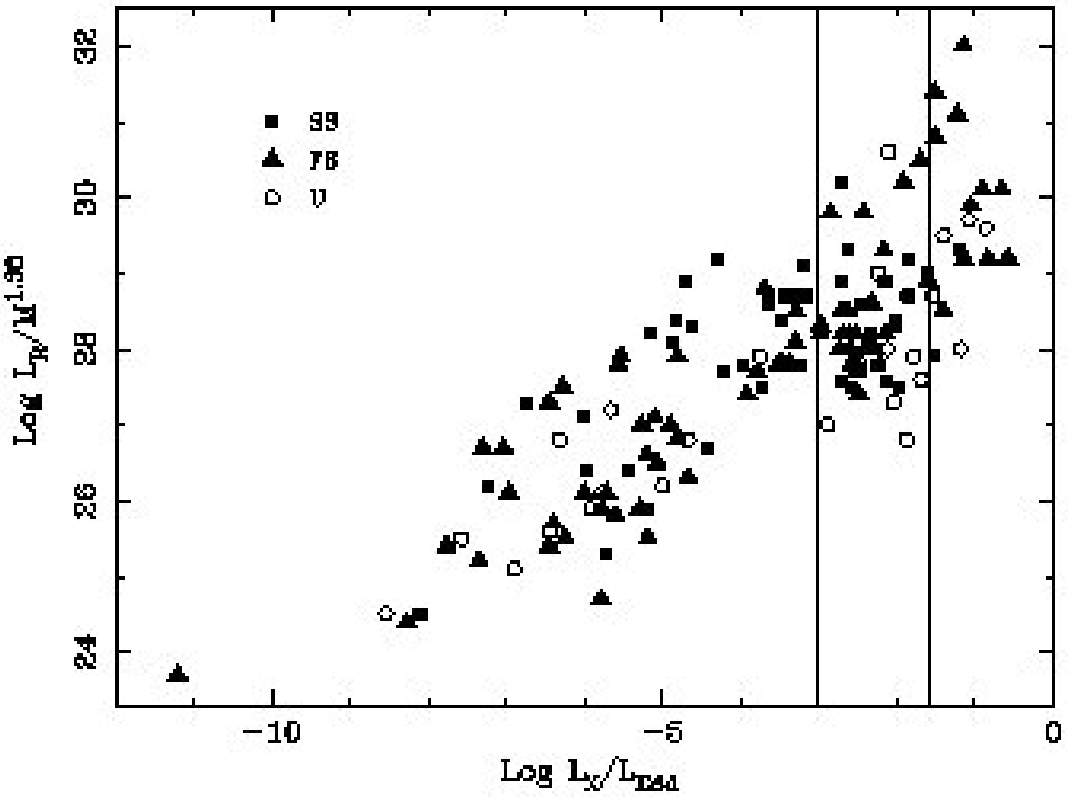

Figure 7. The radio luminosity log L_R, divided by $M^{1.38}$ as a function of the ratio L_X/L_{Edd}. Solid squares are for steep spectrum sources, solid triangles for flat spectrum ones and open circles for sources with undetermined radio spectral index. Two vertical lines mark the boundary of the region where we expect the critical luminosity for the mode change between radiatively inefficient and efficient accretion. The scaling for the radio luminosity with mass is obtained directly from the Fundamental Plane equation (5) by imposing that the X-ray luminosity scales linearly with black hole mass.

Merloni et al. '03

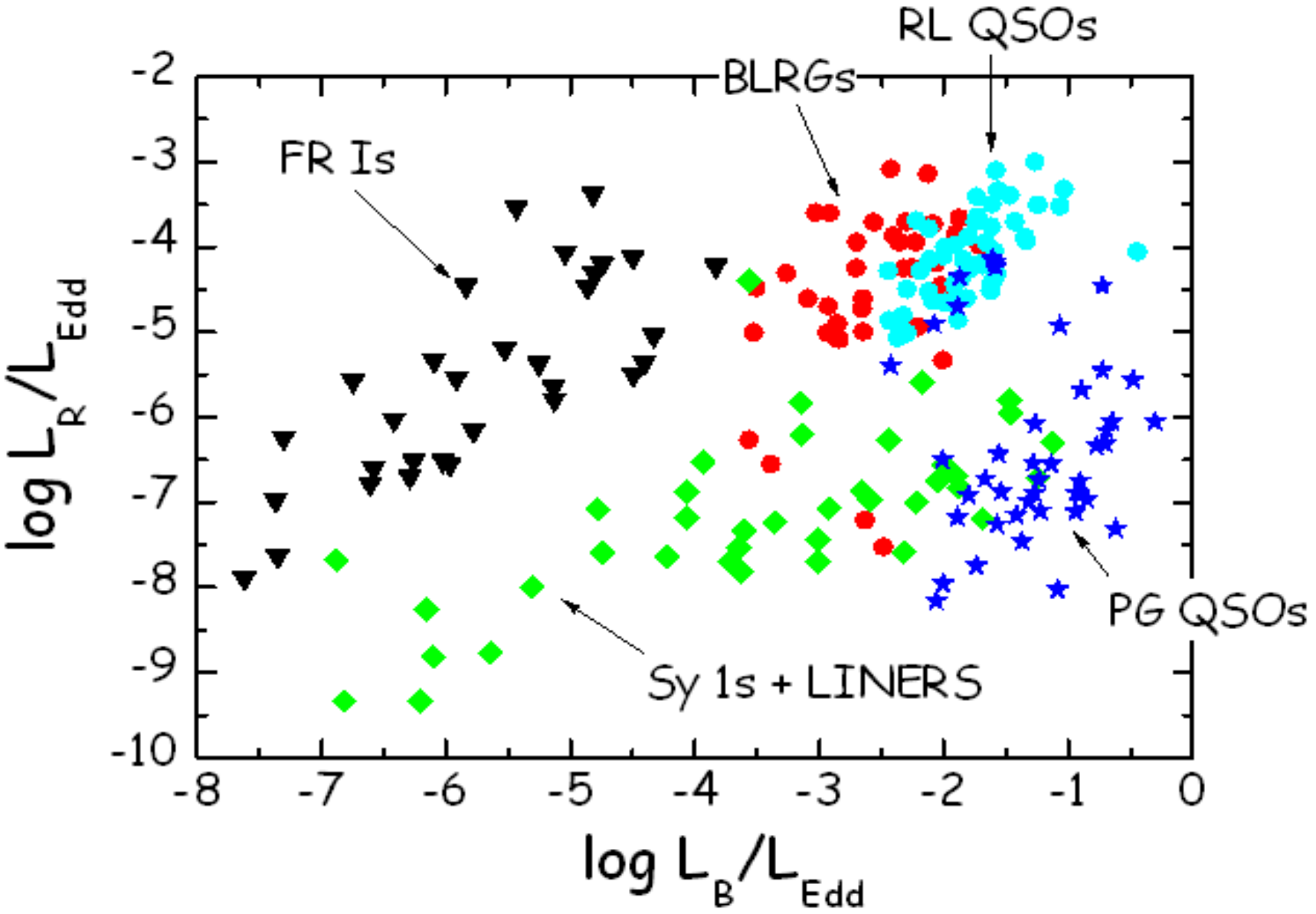

Sikora et al. '07

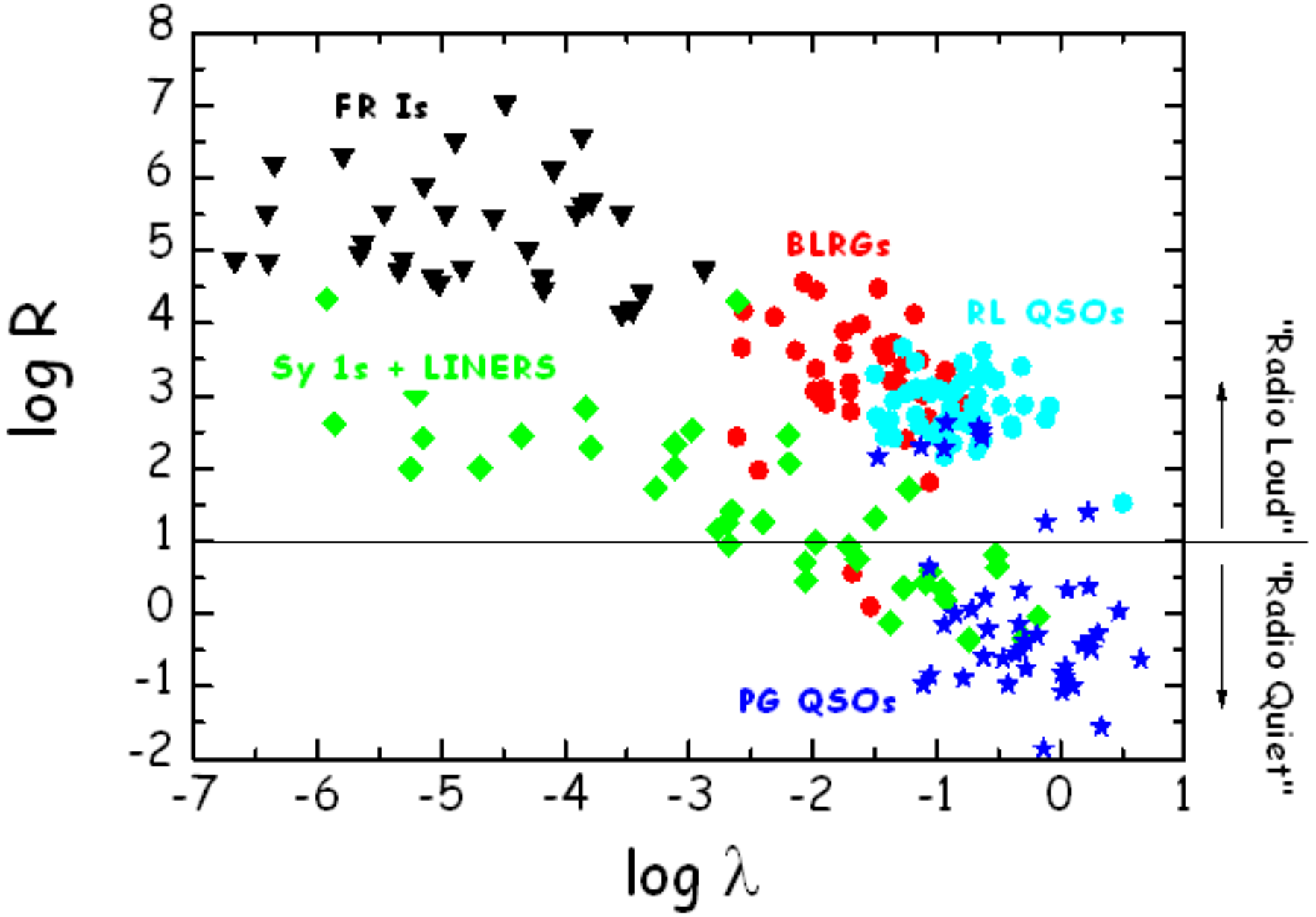
log R
log λ
FR Is
BLRGs
RL QSOs
Sy 1s + LINERS
PG QSOs
"Radio Loud"
"Radio Quiet"
8
7
6
5
4
3
2
1
0
-1
-2
-7
-6
-5
-4
-3
-2
-1
0
1

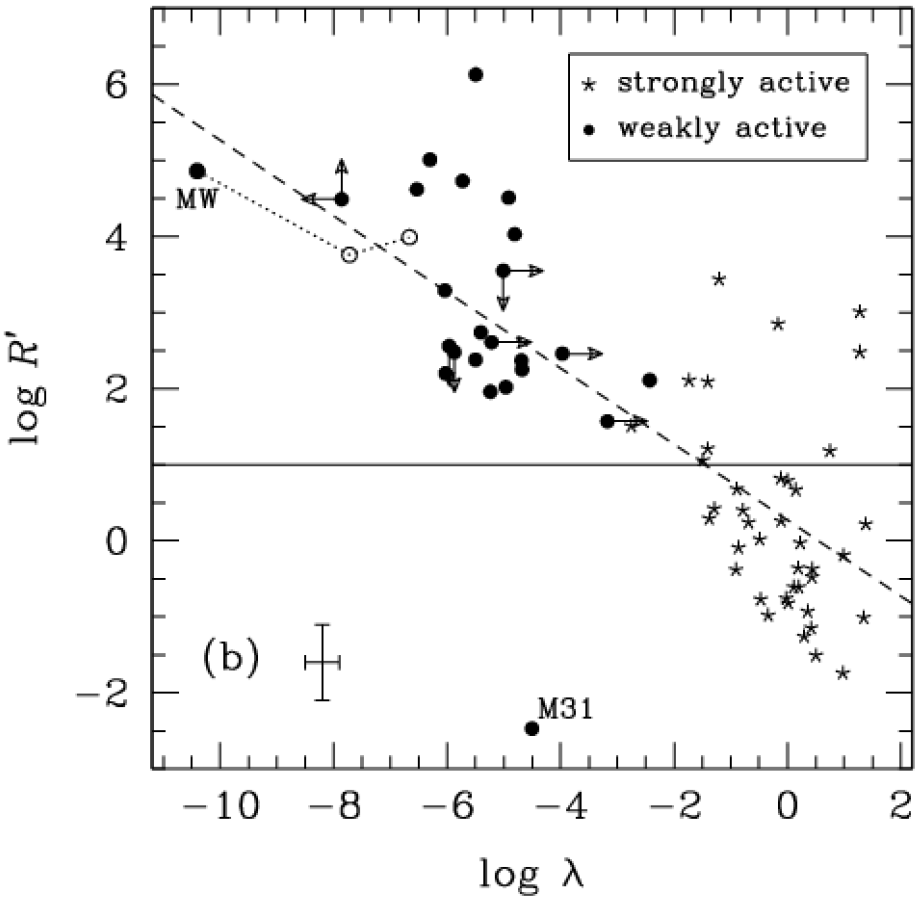
strongly active
weakly active
MW
M31
(b)
log R′
log λ
6
4
2
0
−2
−10
−8
−6
−4
−2
0
2

Ho '02

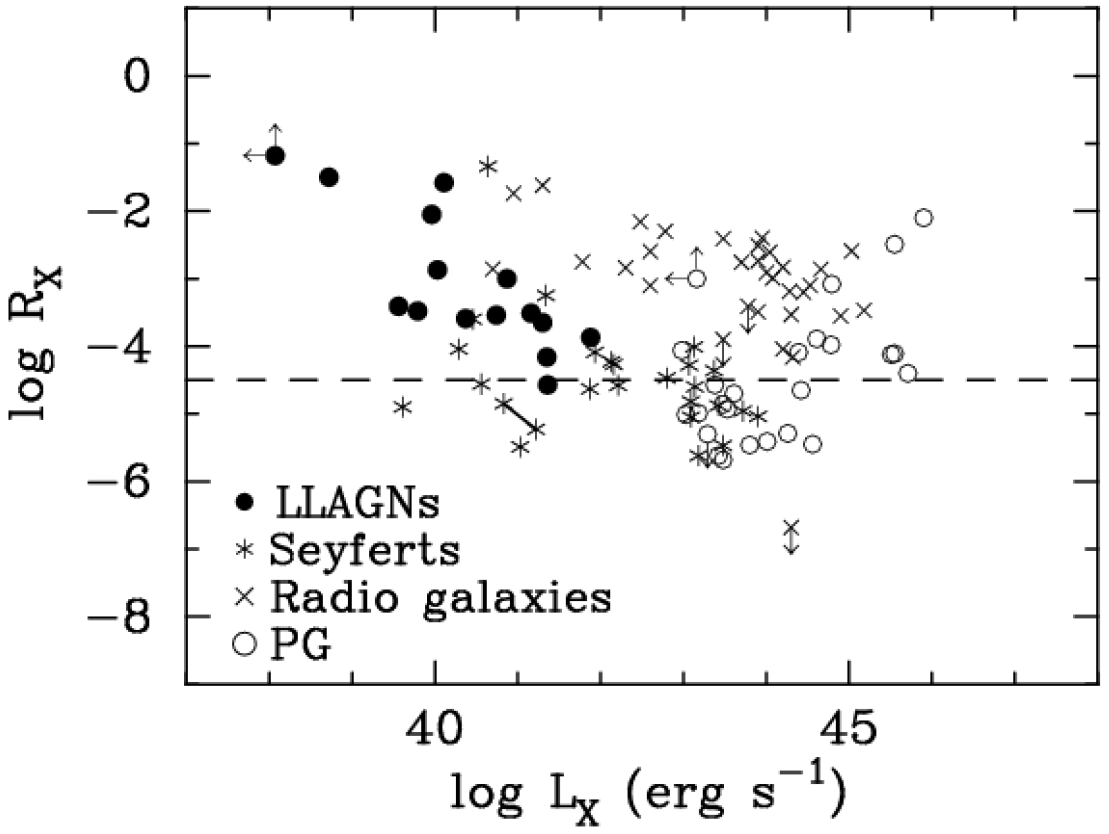

Terashima & Wilson '03

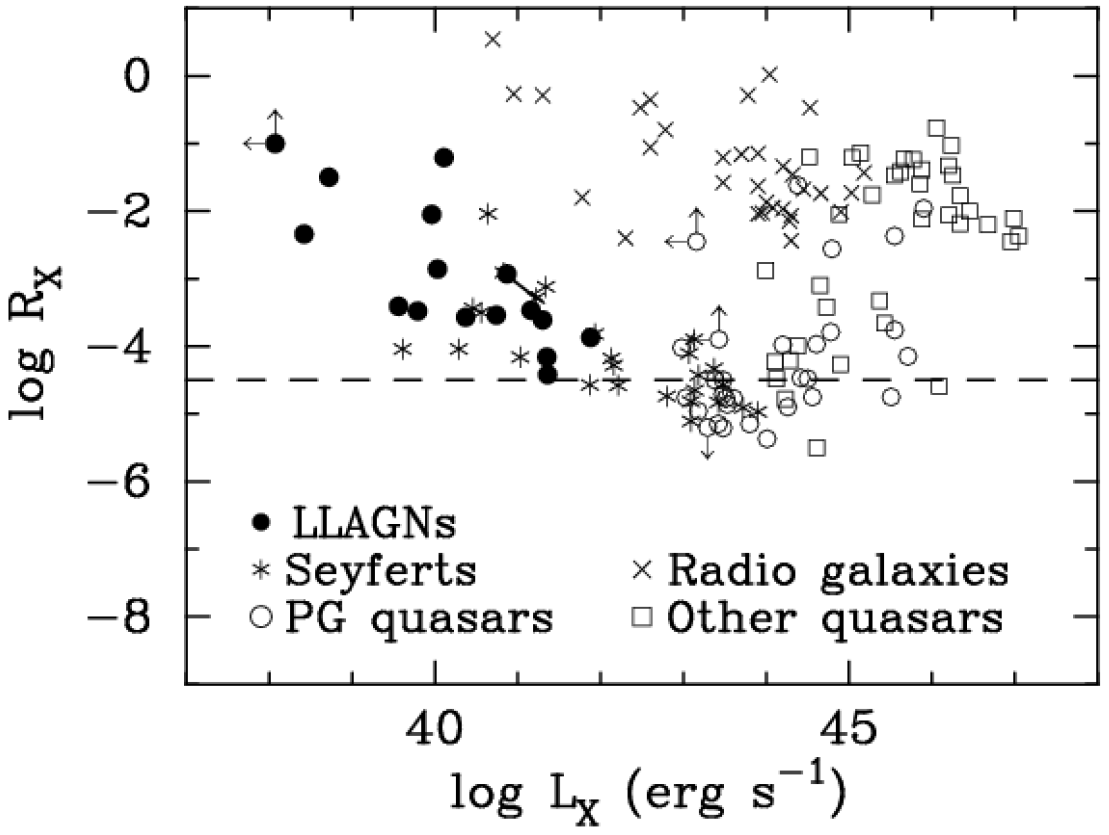

Tershima & Wilson '03

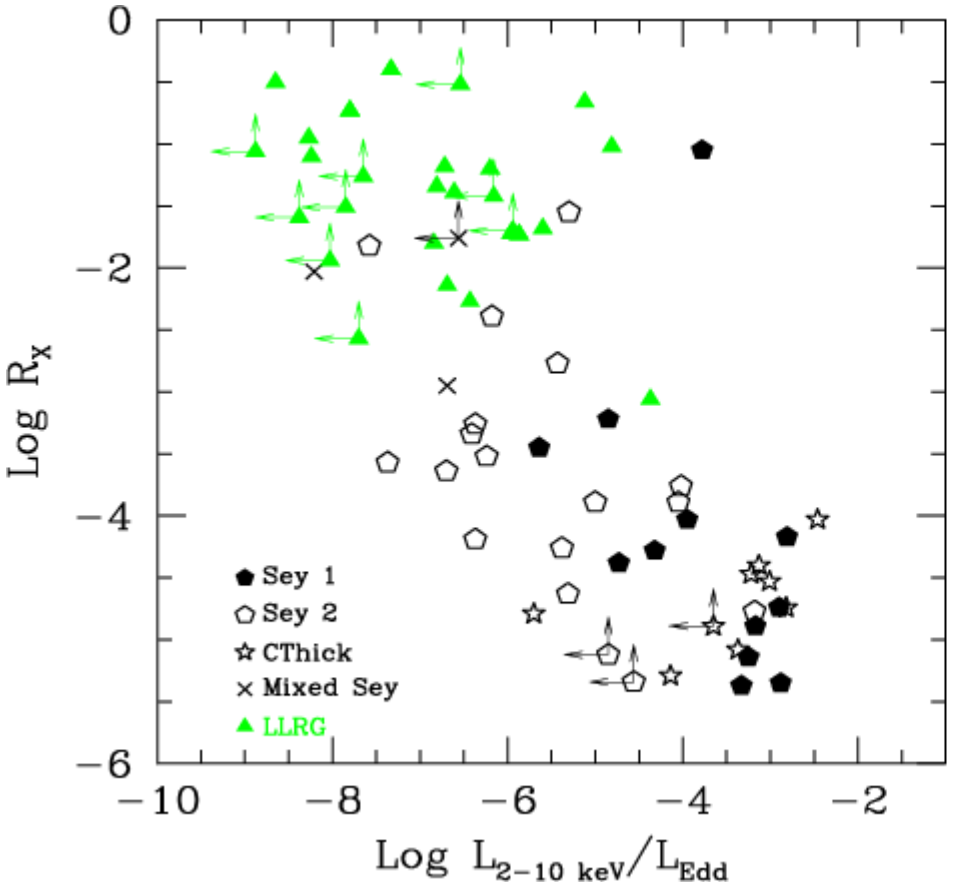

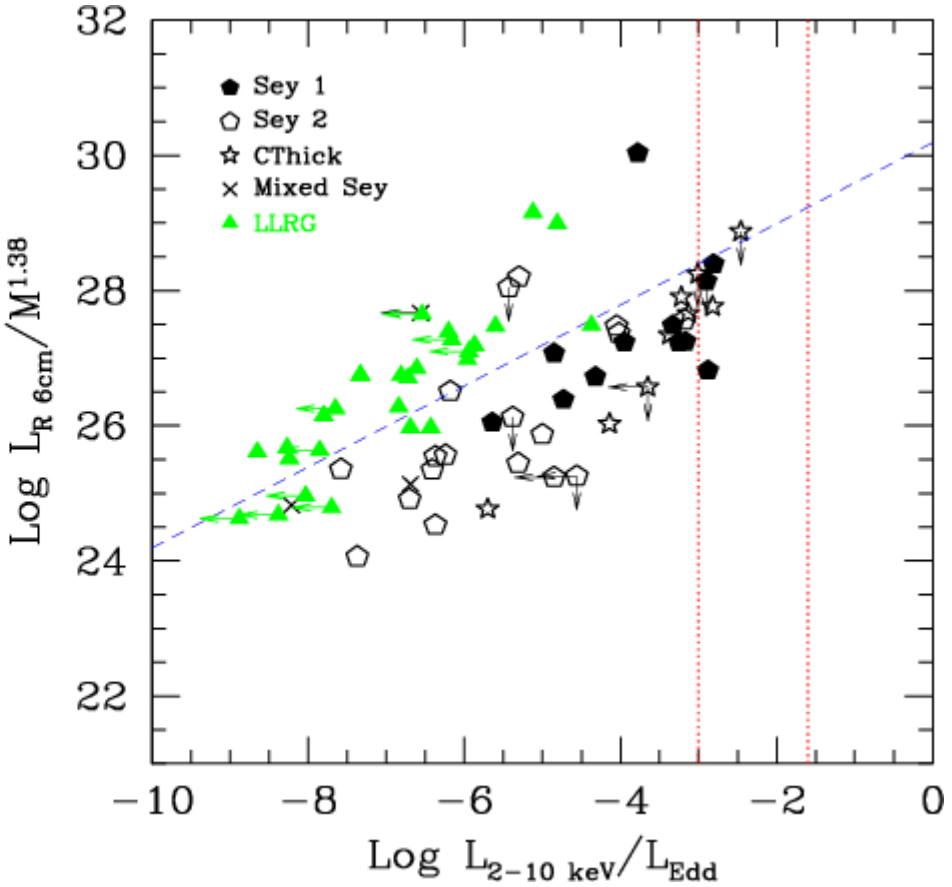

Panessa et al. '07

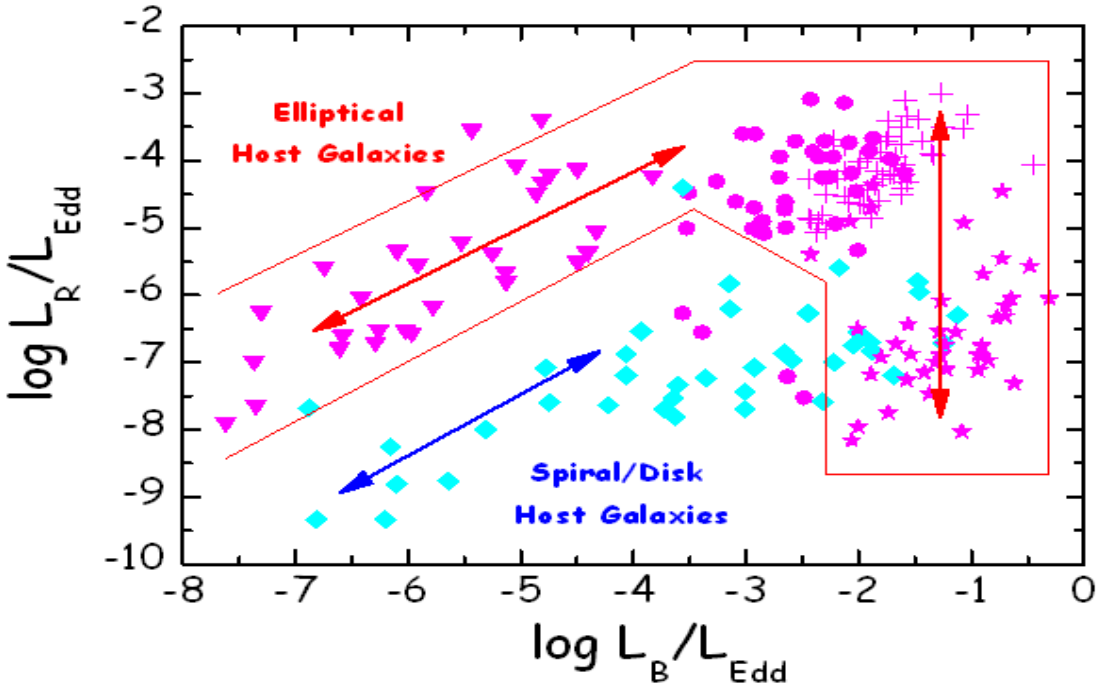
Elliptical
Host Galaxies
Spiral/Disk
Host Galaxies
log L_R/L_Edd
log L_B/L_Edd
-2
-3
-4
-5
-6
-7
-8
-9
-10
-8
-7
-6
-5
-4
-3
-2
-1
0

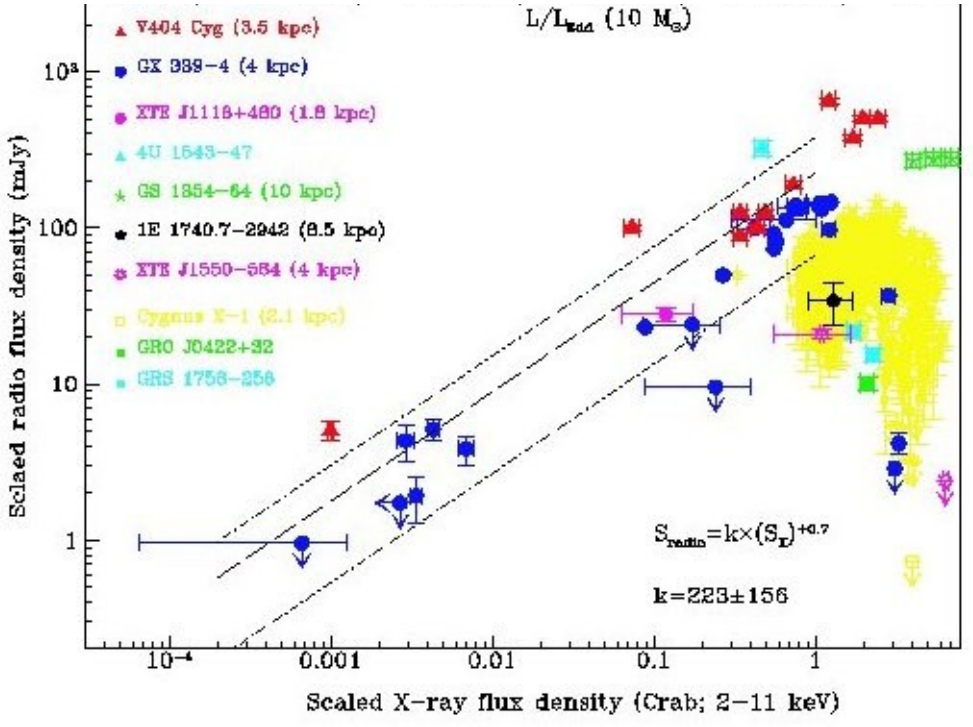
V404 Cyg (3.5 kpc)
GX 339−4 (4 kpc)
XTE J1118+480 (1.8 kpc)
4U 1543−47
GS 1354−64 (10 kpc)
1E 1740.7−2942 (8.5 kpc)
XTE J1550−564 (4 kpc)
Cygnus X−1 (2.1 kpc)
GRO J0422+32
GRS 1758−258
L/L_Edd (10 M_⊙)
S_radio=k×(S_X)^+0.7
k=223±156
Scaled radio flux density (mJy)
Scaled X-ray flux density (Crab; 2−11 keV)
10³
100
10
1
10⁻⁴
0.001
0.01
0.1
1

Jet production efficiency

- $\dot{m}$ + accretion history ?
- $\dot{m}$ + environment ?
- $\dot{m}$ + BH spin ?

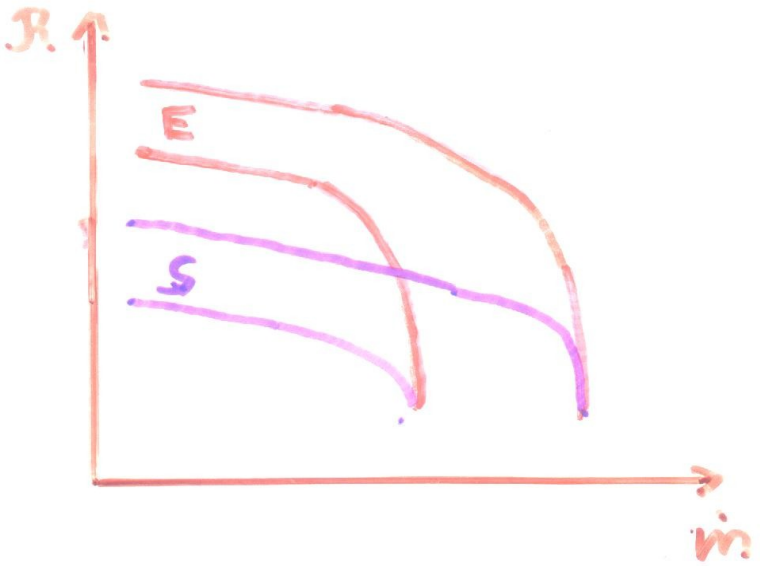

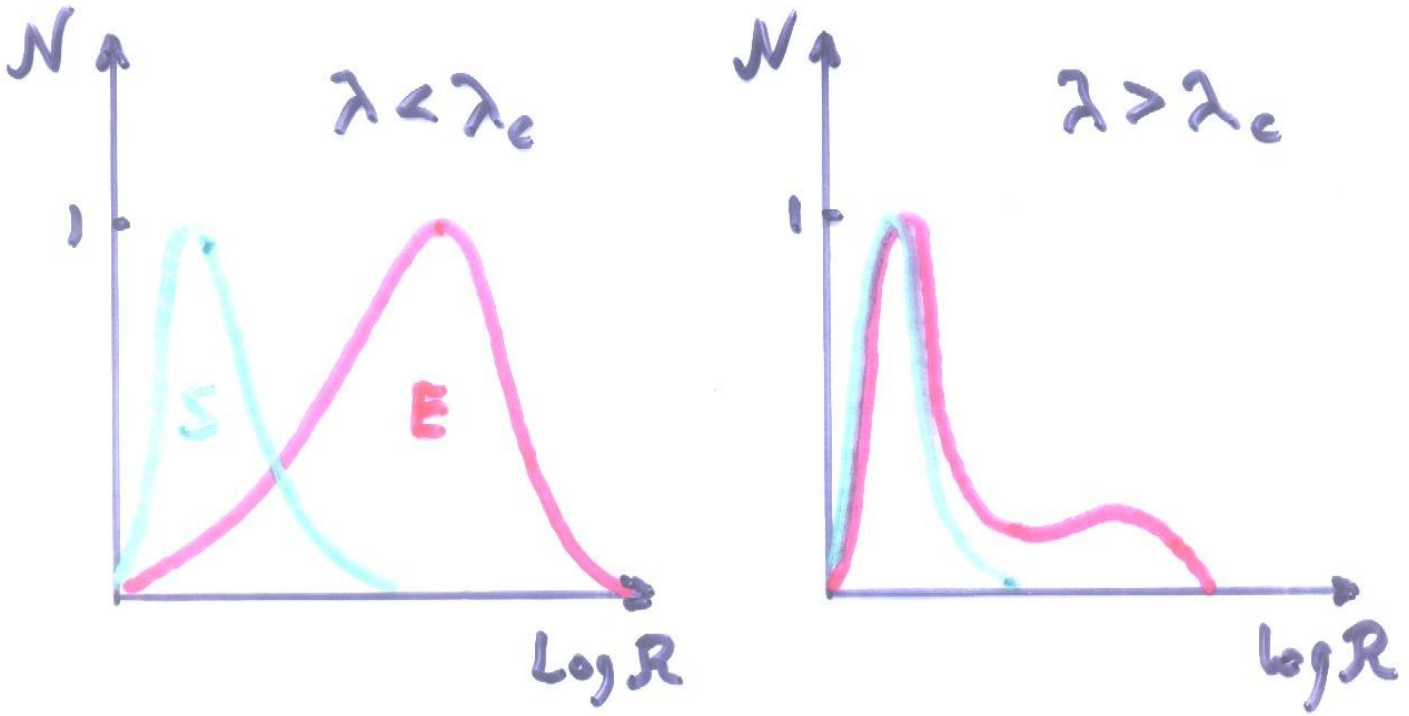

- Why BH have larger spins in Ellipticals than in Spirals?
- How to get switches between radio-loud and radio-quiet states within the spin paradigm framework?

Spin Evolution

- BH mergers
- Accretion
- BZ mechanizm
- Lense-Thirring torque

Refs.: Lense & Thirring '18; Bardeen '70; Wilkins '72; Thorn '74; Bardeen & Petterson '75; Blandford & Znajek '77; Rees '78; Begelman, Blandford & Rees '80; Papaloizou & Pringle '83; Wilson & Colbert '95 Scheuer & Feiler '96; Moderski & Sikora '96,'97; Moderski, Sikora & Lasota '98; Natarajan & Pringle '98 Hughes & Blandford '03; Volonteri, Madau, Quataert & Rees '05; King, Lubow, Ogilvie & Pringle '05

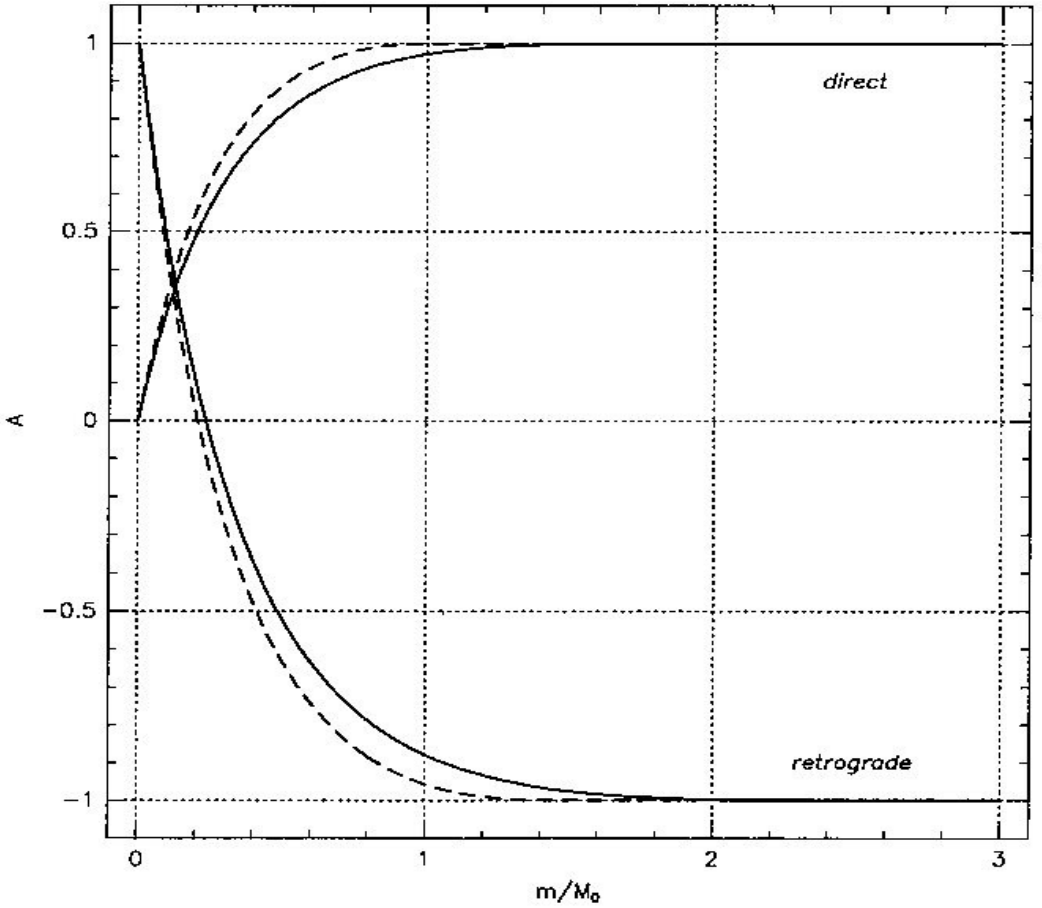

Fig. 1. Evolution of the black hole's angular momentum due to accreted mass. Solid lines are for accretion from a geometrically thin disk, while dashed lines are for accretion from a geometrically thick disk

Moderski & MS '96

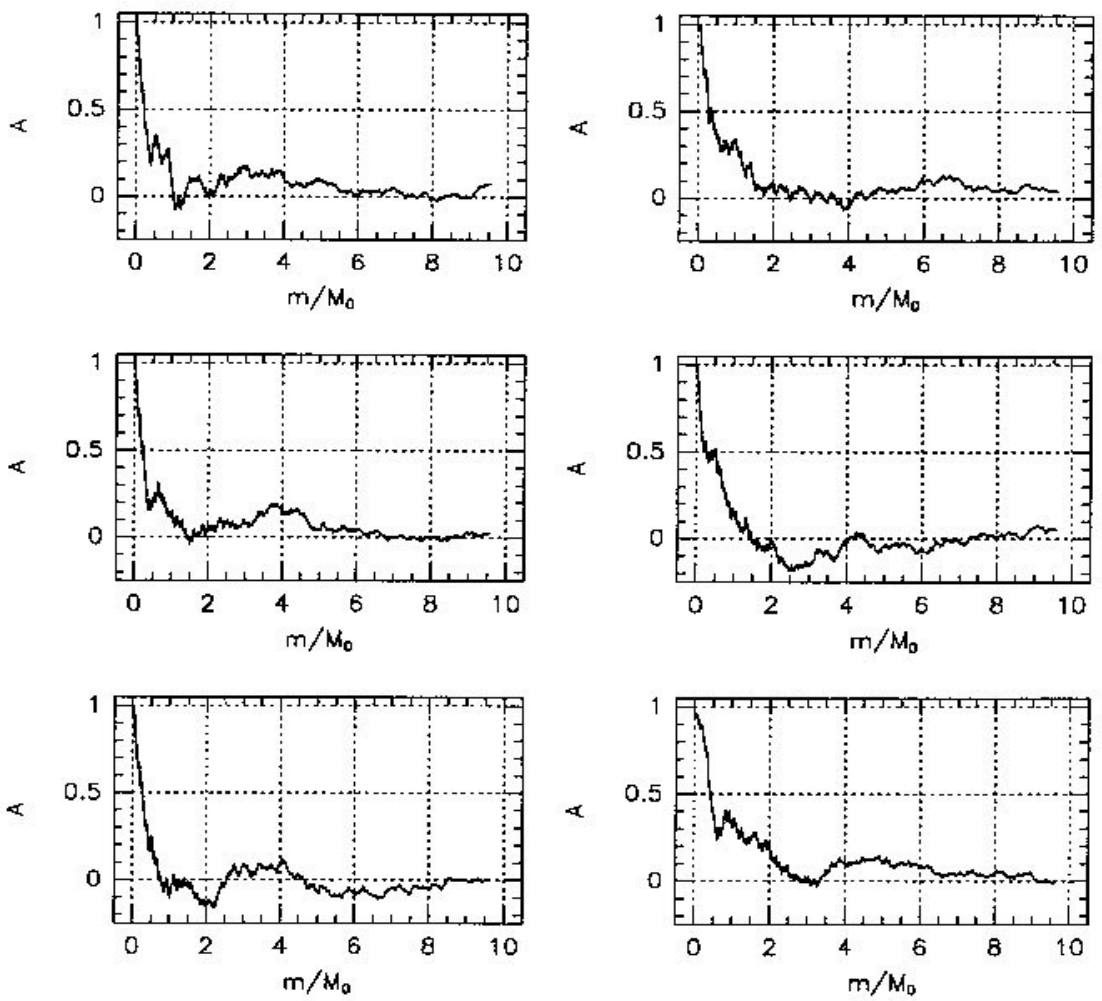

Fig. 2. The angular momentum evolution of a black hole for $A_0 = 1$ and $\Delta m = 0.01 M_0$

Moderski & MS '96

Alingment

$$t_{align} \sim \frac{M_h}{\dot{M}} a \left(\frac{R_g}{R_w}\right)^{\frac{1}{2}}$$

$$\boxed{\frac{m}{M_h} > a \left(\frac{R_g}{R_w}\right)^{\frac{1}{2}}}$$

where $m = \dot{M} \cdot t_{align}$

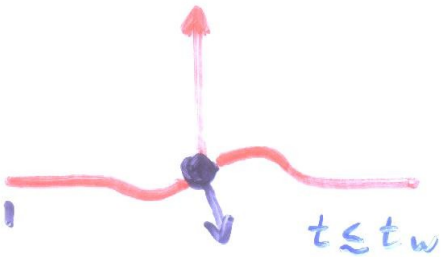

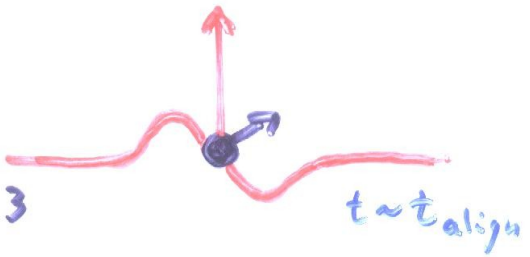

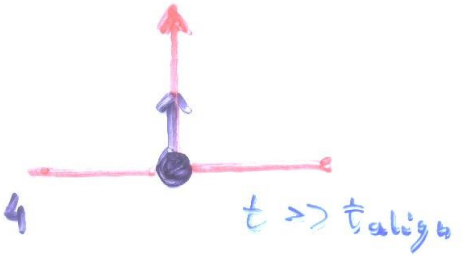

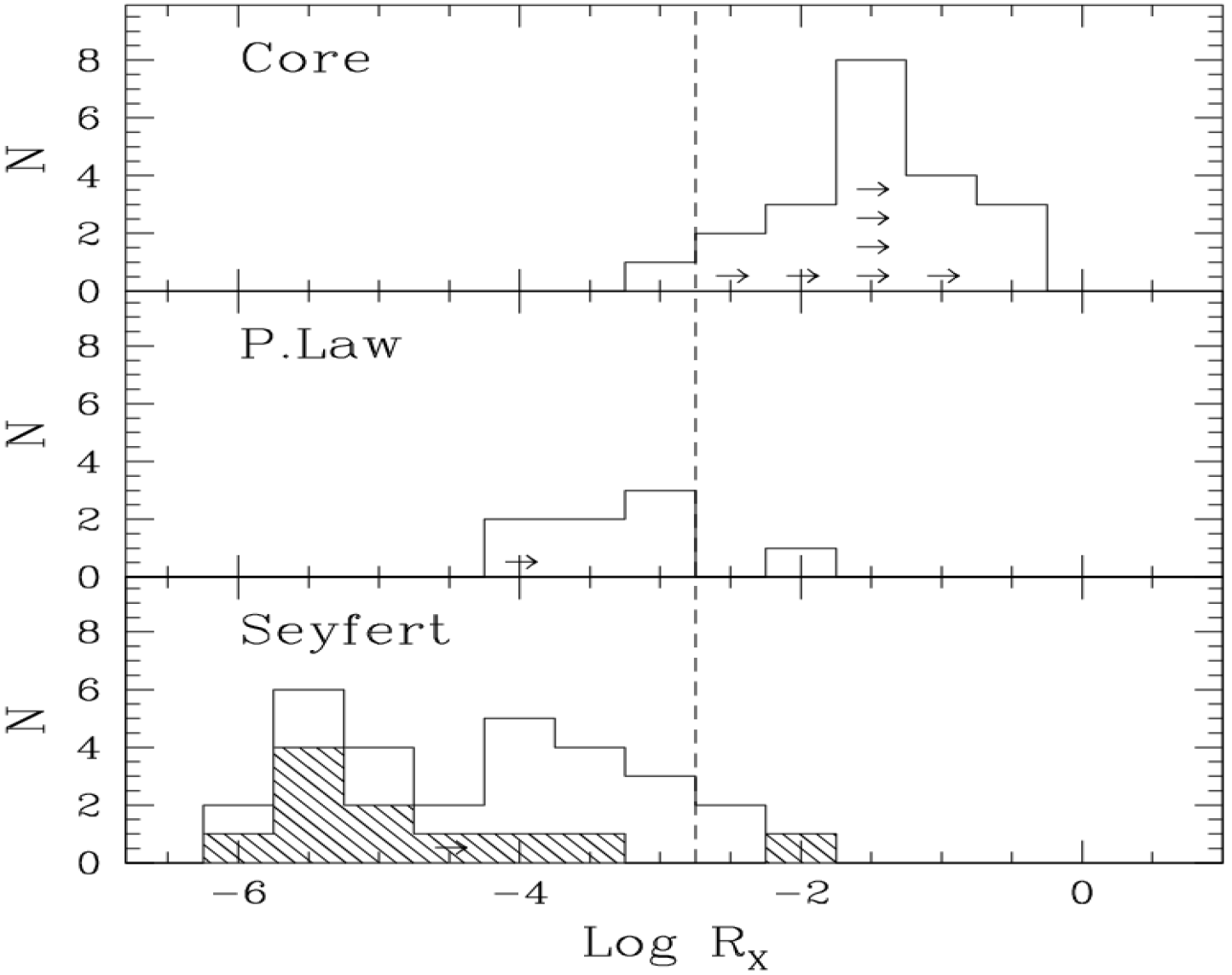

Capetti & Balmaverde '07

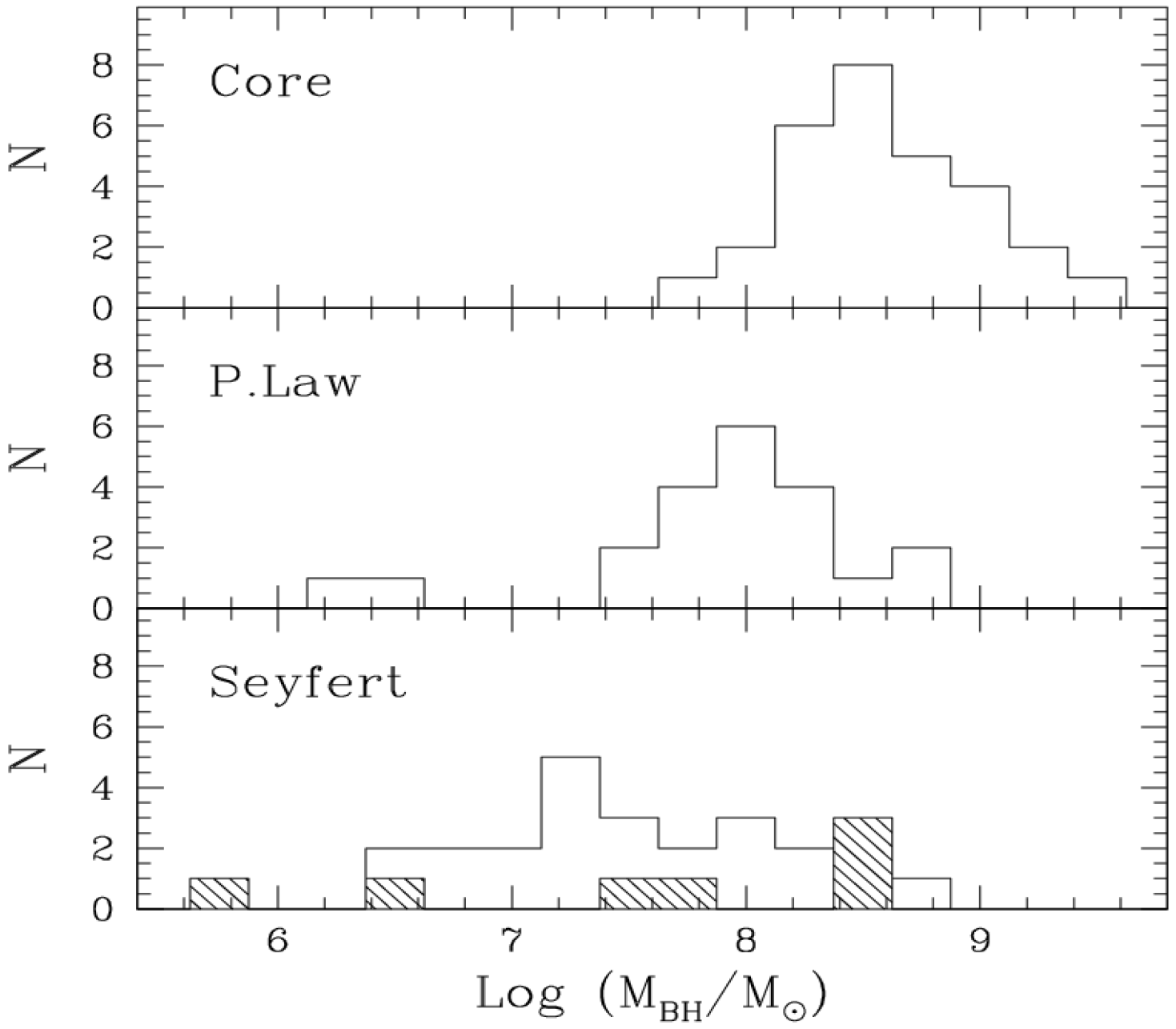

Capetti & Balmaverde '07

Main challenges

- $m/M_h \ll 1$ in spiral galaxies
- $q \sim 1$ in MCG-6-30-15 ?
- $L_p \gg L_e$ in jets (blazars, CP)
- relativistic jets in NS
- jets with $L_j \sim L_{Edd}$